

Death Domain Assembly Mechanism Revealed by Crystal Structure of the Oligomeric PIDDosome Core Complex

Hyun Ho Park,¹ Emmanuelle Logette,² Stefan Raunser,³ Solange Cuenin,² Thomas Walz,³ Jurg Tschopp,² and Hao Wu^{1,*}

¹Weill Medical College and Graduate School of Medical Sciences of Cornell University, New York, NY 10021, USA

²Department of Biochemistry, University of Lausanne, CH-1066 Epalinges, Switzerland

³Department of Cell Biology, Harvard Medical School, Boston, MA 02115, USA

*Correspondence: haowu@med.cornell.edu

DOI 10.1016/j.cell.2007.01.019

SUMMARY

Proteins of the death domain (DD) superfamily mediate assembly of oligomeric signaling complexes for the activation of caspases and kinases via unknown mechanisms. Here we report the crystal structure of the PIDD DD and RAIDD DD complex, which forms the core of the caspase-2-activating complex PIDDosome. Although RAIDD DD and PIDD DD are monomers, they assemble into a complex that comprises seven RAIDD DDs and five PIDD DDs. Despite the use of an asymmetric assembly mechanism, all DDs in the complex are in quasi-equivalent environments. The structure provided eight unique asymmetric interfaces, which can be classified into three types. These three types of interactions together cover a majority of the DD surface. Mutagenesis on almost all interfaces leads to disruption of the assembly, resulting in defective caspase-2 activation. The three types of interactions may represent most, if not all, modes of interactions in the DD superfamily for assembling complexes of different stoichiometry.

INTRODUCTION

The death domain (DD) superfamily comprises the death domain (DD) subfamily, the death effector domain (DED) subfamily, the caspase recruitment domain (CARD) subfamily, and the pyrin domain (PYD) subfamily. It is one of the largest protein domain superfamilies (Kohl and Grutter, 2004; Park et al., 2007; Reed et al., 2004). These domains mediate homotypic interactions within each subfamily and play critical roles in the formation of oligomeric signaling complexes, such as the death-inducing signaling complex (DISC) assembled by some members of the

TNF receptor family for caspase-8 and caspase-10 activation, the apoptosome for caspase-9 activation, the inflammasome for caspase-1 activation, and the PIDDosome for caspase-2 activation (Kohl and Grutter, 2004; Park et al., 2007; Reed et al., 2004). These domains also participate in the assembly of signaling complexes for kinase and NF- κ B activation in TNF signaling, T cell and B cell receptor signaling, intracellular pathogen sensing and defense, and response to DNA damage (Kohl and Grutter, 2004; Park et al., 2007; Reed et al., 2004).

The DD superfamily domains appear to mediate two types of functions in these oligomeric signaling complexes for caspase and kinase activation. One function is to mediate the assembly of oligomeric platforms for these complexes, and the other is to recruit downstream effectors. In a simplified view, these molecular complexes activate their effectors via proximity-induced autoactivation, such as dimerization, proteolytic processing and transphosphorylation. For caspases, proximity-induced dimerization is sufficient for their activation (Baliga et al., 2004; Pop et al., 2006; Yin et al., 2006).

The unifying feature of the DD superfamily is the six-helical bundle structural fold, as first revealed by NMR structures of Fas DD, FADD DED, RAIDD CARD, and NALP1 PYD (Kohl and Grutter, 2004; Park et al., 2007; Reed et al., 2004). There are currently two complex structures in the DD superfamily that are involved in effector recruitment, the Pelle DD:Tube DD complex involved in *Drosophila* Toll signaling (Xiao et al., 1999) and the Apaf-1 CARD:procaspase-9 CARD complex involved in caspase-9 activation (Qin et al., 1999). Despite the fundamental importance of the DD superfamily in apoptotic and immune signaling pathways, no structures of any oligomeric DD superfamily complexes are currently available.

Caspase-2 is an initiator caspase and the most evolutionarily conserved caspase (Lassus et al., 2002; Wang et al., 1994). Caspase-2-deficient germ cells and oocytes are resistant to cell death after treatment with chemotherapeutic agents (Bergeron et al., 1998). In response to DNA damage, caspase-2 acts upstream of the mitochondria by inducing Bid cleavage, Bax translocation, and

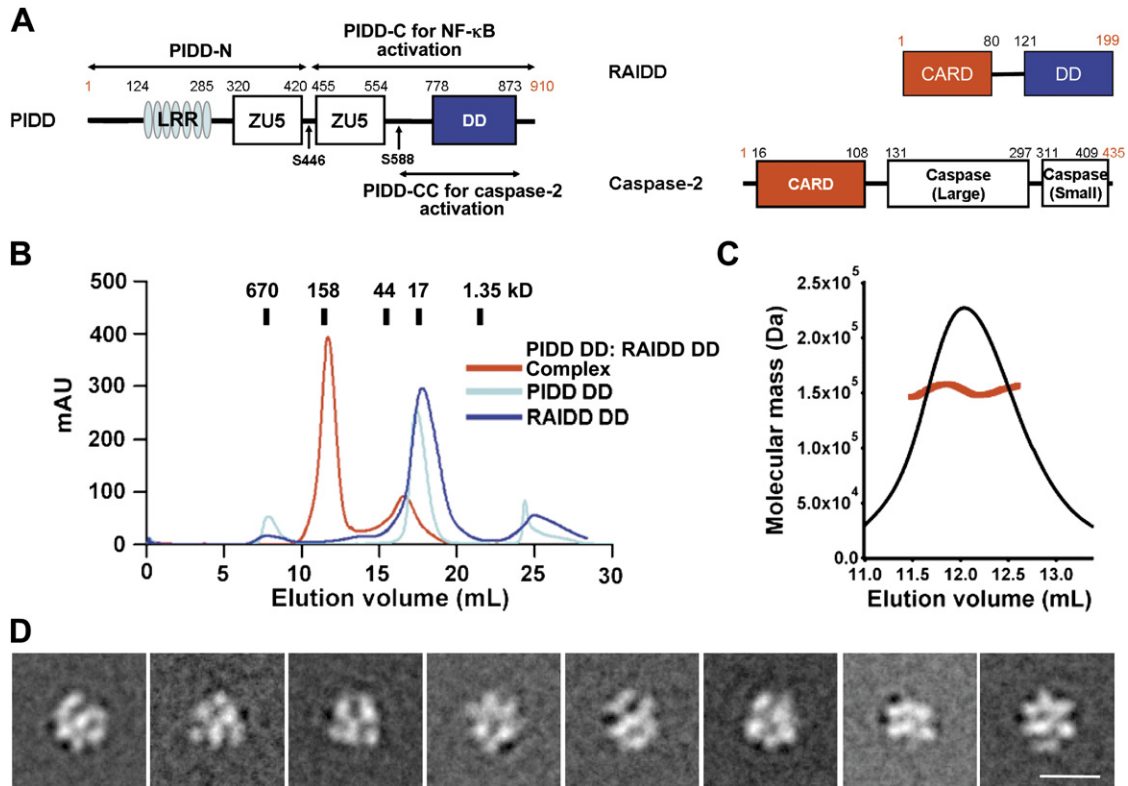


Figure 1. Characterization of the PIDD DD:RAIDD DD Complex

(A) Domain organizations of the PIDDosome components, PIDD, RAIDD, and caspase-2. The cleavage fragments of PIDD are shown. (B) Gel filtration profiles of PIDD DD alone (cyan), RAIDD DD alone (blue), and the complex (red). (C) Determination of the molar mass of the complex by multi-angle light scattering. (D) Representative class averages obtained with negatively stained sample. Each class contains 50 to 170 particles. Scale bar, 10 nm.

cytochrome c release (Guo et al., 2002; Lassus et al., 2002; Robertson et al., 2002). When added to purified mitochondria, caspase-2 leads to cytochrome c release (Guo et al., 2002; Robertson et al., 2002).

The PIDDosome for caspase-2 activation is composed of three components, PIDD (Lin et al., 2000; Tellerie et al., 2000a), RAIDD (Duan and Dixit, 1997), and caspase-2 (Tinel and Tschopp, 2004) (Figure 1A). It is assembled via a DD:DD interaction between RAIDD and PIDD and a CARD:CARD interaction between RAIDD and caspase-2. Not only is PIDD DD essential for the activation of caspase-2, but it can also interact with the DD of RIP1, a kinase implicated in the activation of NF- κ B (Janssens et al., 2005). PIDD appears to act as a molecular switch, controlling the balance between life and death upon DNA damage (Janssens et al., 2005).

Full-length PIDD contains 910 residues with seven leucine-rich repeats (LRRs), two ZU-5 domains, and a C-terminal DD (Figure 1A). It is often autoprocessed via an intein-like mechanism into shorter fragments of 51 kDa, 48 kDa, and 37 kDa (Pick et al., 2006; Tinel et al., 2007; Tinel and Tschopp, 2004). The cleavage sites have been mapped to S446 and S588 (Tinel et al., 2007). Cleav-

age at S446, which locates in between the two ZU-5 domains, generates a PIDD-N fragment of 48 kDa (residues 1–445) and a PIDD-C fragment of 51 kDa (residues 446–910). Further cleavage at S588, which locates in between the second ZU-5 domain and the C-terminal DD, generates a PIDD-CC fragment of 37 kDa (residues 588–910). Autocleavage of PIDD determines the outcome of the downstream signaling events. The initially formed PIDD-C fragment mediates the activation of NF- κ B via the recruitment of RIP1 and NEMO, and the subsequent formation of PIDD-CC causes caspase-2 activation and cell death (Tinel et al., 2007) (Figure 1A). Full-length PIDD is not active in either NF- κ B or caspase-2 activation.

PIDD-CC containing the C-terminal DD is sufficient for PIDDosome formation and caspase-2 activation (Tinel et al., 2007). In addition, PIDD DD alone is sufficient in sensitizing a colon carcinoma cell line for UV-induced apoptosis (Pick et al., 2006) and in formation of a ternary complex with RAIDD and caspase-2 CARD upon overexpression in 293T cells (Tinel and Tschopp, 2004). The PIDD DD:RAIDD DD complex forms the core oligomeric platform in PIDDosome, while the RAIDD CARD:caspase-2 CARD interaction is responsible for caspase-2 recruitment.

To elucidate the molecular basis of caspase-2 activation and of the assembly mechanisms of the DD superfamily, we determined the crystal structure of the PIDD DD:RAIDD DD complex, which comprises seven RAIDD DD and five PIDD DD molecules. Despite the use of an asymmetric assembly mechanism, all DDs in the complex are in quasi-equivalent environments. The structure provided multiple observations of eight unique asymmetric interfaces, which can be further classified into three types. These interactions can coexist on a single DD and together cover a majority of the DD surface. Structure-based mutagenesis on almost all interfaces leads to disruption of the assembly, resulting in defective caspase-2 activation. In contrast to the concept that DD superfamily interactions may involve any available surfaces and may be very diverse, we show here that the three types of interactions in this complex may represent most, if not all, modes of interactions in the DD superfamily and may be used to assemble oligomeric complexes of different stoichiometry.

RESULTS

Overall Structure of the PIDD DD:RAIDD DD Complex, the Core Oligomerization Platform of the PIDDosome

As a first step toward elucidating the molecular basis of PIDDosome formation, we expressed and purified the DDs of PIDD and RAIDD. Although PIDD DD and RAIDD DD are both monomeric in solution, when mixed together, the complex containing both DDs eluted at ~ 150 kDa from a Superdex 200 gel filtration column (Figure 1B). Because both mass and shape affect gel filtration positions, we further used multi-angle light scattering (MALS) with refractive index to accurately measure its molecular mass. MALS measurement gave a molecular mass of 152.4 kDa (0.8% fitting error) for the complex, with a polydispersity of 1.001 (Figure 1C). These data suggest that PIDD DD and RAIDD DD assemble into an oligomeric complex.

Electron microscopy (EM) of the negatively stained PIDD DD:RAIDD DD complex revealed a monodisperse and homogeneous particle population (Figure S1 in the Supplemental Data available with this article online). Classification of 3708 particle images into 25 groups produced class averages that depicted molecules of similar size, about 9 nm in diameter, but with varying structural features (Figure 1D; Figure S1). The differences in the projections most likely arise from different orientations, in which the complex had adsorbed to the carbon support film.

We crystallized the complex and determined its structure at 3.2 Å resolution using single-wavelength anomalous diffraction of a mercury derivative (Table 1). The structure revealed that the PIDD DD:RAIDD DD complex contains five PIDD DD and seven RAIDD DD molecules. It forms a compact globular structure of approximately 90 Å in diameter (Figures 2A and 2B). The globular shape of the structure is consistent with the normal elution behavior of the complex in gel filtration. This size agrees

well with the EM images. In addition, despite the strong contrast between the individual domains in the EM projection averages due to stain accumulation, comparison of the experimental class averages with projections calculated from the atomic model and resolution filtered to 30 Å clearly showed that the class averages depict the same complex. The differences between the class averages arise from different orientations in which the complex had adsorbed to the carbon support film (Figure S1). As the calculated molecular weights of monomeric PIDD DD and RAIDD DD are 13,036 Da and 13,075 Da, respectively, the calculated molecular mass of a 5:7 PIDD DD:RAIDD DD complex is 156.7 kDa, which agrees well with the molecular mass measured by MALS.

PIDDosome for caspase-2 activation contains the PIDD autoprocessing fragment PIDD-CC, RAIDD, and caspase-2 (Tinel et al., 2007; Tinel and Tschopp, 2004), with calculated molecular weights of 36,560 Da, 22,745 Da, and 50,685 Da, respectively. If the same PIDD DD:RAIDD DD stoichiometry is present in the PIDDosome for caspase-2 activation, the calculated molecular mass of the PIDDosome with five PIDD-CC, seven RAIDD, and seven caspase-2 molecules would be 696.8 kDa. This molecular mass is in striking agreement with gel filtration analysis of the PIDDosome, which showed a molecular mass of ~ 670 kDa (Read et al., 2002; Tinel and Tschopp, 2004).

The structure of the PIDD DD:RAIDD DD complex may be divided into three layers viewing from the side of the complex, two RAIDD DDs at the top layer (R6 and R7), five RAIDD DDs in the middle layer (R1–R5), and five PIDD DDs at the bottom layer (P1–P5) (Figure 2A). Viewing from the top of the complex, the middle and the bottom layers form two stacked closed rings (Figures 2B and 2C). The termini of the DDs point to the periphery of the complex (Figures 2B and 2C). The peripheral locations of the N termini allow PIDD DD to connect to the N-terminal region of PIDD-CC and RAIDD DD to connect to its CARD domain (Figure 2D). Therefore, one could envision that the PIDD DD:RAIDD DD complex localizes in the center of the PIDDosome to mediate oligomerization, while the N-terminal region of PIDD-CC, RAIDD CARD, and caspase-2 occupy the outer part of the PIDDosome. In this scenario, the seven caspase-2 molecules in the complex are brought into proximity for their dimerization and activation (Figure 2D).

The PIDD DD:RAIDD DD Complex Is Constructed by Successive Screw Rotations

Strikingly, the core complex of five PIDD DDs and five RAIDD DDs does not possess a recognizable symmetry. Looking down from the top, the RAIDD DDs and the PIDD DDs around the two stacked rings are related by rotations around a common central axis (Figure 2C; Figure S2). Pairwise superposition showed that the molecules are related by two different rotation angles at different locations (Figure 2C). In addition, viewing from the side of the complex, the DDs in each layer are not localized on

Table 1. Crystallographic Statistics

	Mercury Derivative	Native
Data collection		
Beamline	X4A of NSLS	NE-CAT of APS
Space group	P6 ₅	P6 ₅
Cell dimensions (a, b, c)	138.9 Å, 138.9 Å, 208.3 Å	138.4 Å, 138.4 Å, 207.5 Å
Resolution	30–4.0 Å	30–3.2 Å
R _{sym}	7.5% (42.8%)	7.4% (36.4%)
I/σ	29.7 (3.2)	40.5 (2.1)
Completeness	100% (100%)	97.7% (79.4%)
Redundancy	5.7 (5.7)	10.3 (5.9)
Refinement		
Resolution		30–3.2 Å
No. reflections		34,580
R _{work} /R _{free}		23.6%/27.5%
No. atoms		
Protein/water and other small molecules		9082/19
Average B factors		
Protein/water and other small molecules		84.5 Å ² /34.3 Å ²
Root mean square deviations		
Bond lengths/angles		0.01 Å/1.7°
Ramachandran plot		
Most favored/ additionally allowed		85.8%/13.6%

Highest-resolution shell is shown in parenthesis.

the exact same plane within the complex, suggesting that the rotations are screw rotations (Figure 2A; Figure S2).

If we cut open the structure from the side and lay the molecules flat, the locations of the DDs form a staggered hexagonal pattern (Figure 2E). If we take a hypothetical subcomplex of one PIDD DD and one RAIDD DD (PR subcomplex) as a central building block of this pattern, the complex may be described as five successive screw rotations of the PR subcomplex around the central vertical axis. There are two types of such screw rotations in the assembly of the complex, one rotating approximately 84° and translating down the axis and the other rotating approximately 54° and translating up the axis (Figures 2C and 2E). Among the five screw rotations in the complex, three are of 84° and two are of 54°. This gives a total rotation of 84° × 3 + 54° × 2 = 360° and a zero net translation to close the rings. The net translation is zero because each upward translation is 1.5-fold of the downward translation. The top layer molecules R6 and R7 are built above R5 and R2, respectively, and the relationships of R6:R5 and R7:R2 are similar to the R1:P1 relationship.

Massive surface areas in a total of 17,207 Å² are buried upon complex formation, which correspond to an average of 1434 Å² per DD in the complex. With the exception of

the surface from which the N and C termini protrude out, virtually all other surfaces of each DD are used in complex formation.

Despite Lack of Conventional Symmetry, Each DD in the Complex Has a Quasi-Equivalent Environment

Given this unusual assembly mechanism, we investigated whether the different DDs in the complex are surrounded by different environments. We first superimposed the five pairs of PR subcomplexes and found that they align well with pairwise root mean square deviations (RMSD) of below 0.4 Å (Figure 3A). In addition, there is a high degree of structural similarity between RAIDD DD and PIDD DD (Figure 3B). They superimpose to an RMSD of 1.1 Å among 64 aligned Cα atoms. Although it is known that both RAIDD DD and PIDD DD exhibit the same six-helical bundle structure characteristic of the DD superfamily, this level of structural similarity is unexpected, as the sequence identity between the two domains is only 15% (Figure 3D).

As seen from the construction model of the complex, each DD has maximally six immediate neighboring DDs (Figure 2E). Some DDs, such as R2 and R5, have all six neighboring DDs. Other DDs have three to five neighboring

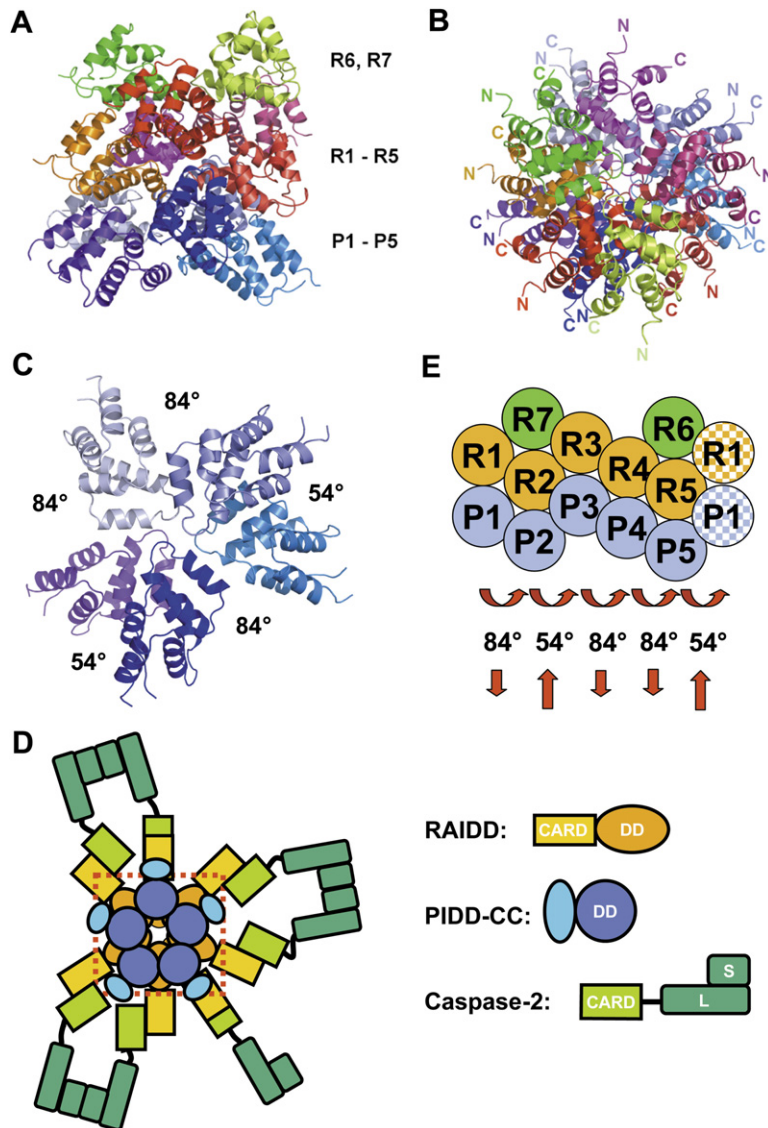


Figure 2. Overview of the PIDD DD:RAIDD DD Complex

(A) Side view of the complex. The top layer contains two RAIDD DD molecules (green and yellow). The middle layer contains five RAIDD DD molecules (red, purple, orange, magenta, and pink). The bottom layer contains five PIDD DD molecules (different shades of blue).

(B) Top view of the complex.

(C) Top view of the five PIDD DDs at the bottom layer, showing the rotational relationships.

(D) A model of the PIDDosome for caspase-2 activation, showing the PIDD DD:RAIDD DD complex inside a dotted red box and the rest of the domains and molecules. Caspase-2 molecules are schematically dimerized to illustrate proximity-induced dimerization in the PIDDosome.

(E) A schematic planar diagram for the construction of the complex, showing the successive screw rotations of a hypothetical PR subcomplex. The shaded R1 and P1 molecules at the right indicate that the rotations have brought the PR subcomplex back to the beginning and completed the ring.

DDs. Strikingly, all DDs in the complex form similar contacts with their respective neighboring DDs. As an example, Figure 3C shows the superposition of R5 and its six neighboring DDs with P1 and its five neighboring DDs. If we take R5 and its neighboring DDs as a standard, all other DDs can be superimposed to this standard along with their respective neighboring DDs (Figure S3), demonstrating that all DDs have an equivalent environment in the complex. Because at the same relative positions around a central DD there may either be a RAIDD DD or a PIDD DD, this equivalent environment is a quasi-equivalent environment.

There Are Eight Kinds of Interfaces in the PIDD DD:RAIDD DD Complex, which May Be Classified into Three Types of Interactions

The different interfaces in the PIDD DD:RAIDD DD complex may be classified into three types based on the regions involved in these interactions (Figure 4A). Because

it has been proposed earlier that DDs may use diverse mechanisms of interactions (Xiao et al., 1999), we were surprised to find that these three types of interactions are similar to the procaspase-9 CARD:Apaf-1 CARD interaction (Qin et al., 1999), the Pelle DD:Tube DD interaction (Xiao et al., 1999), and an interaction proposed to exist in the Fas DD:FADD DD complex (Weber and Vincenz, 2001). Because these interactions have been previously named types I, II, and III, respectively (Weber and Vincenz, 2001), we followed the same convention in our description of the interactions. Depending on whether the interactions are between a RAIDD DD and a PIDD DD (R:P), between two RAIDD DDs (R:R), or between two PIDD DDs (P:P), the type I, II, and III interactions contain three, two, and three subtypes, respectively, making a total of eight kinds of interfaces.

In the type I interaction, residues at H1 and H4 of the first DD (type Ia surface) interact with residues at H2 and H3 of

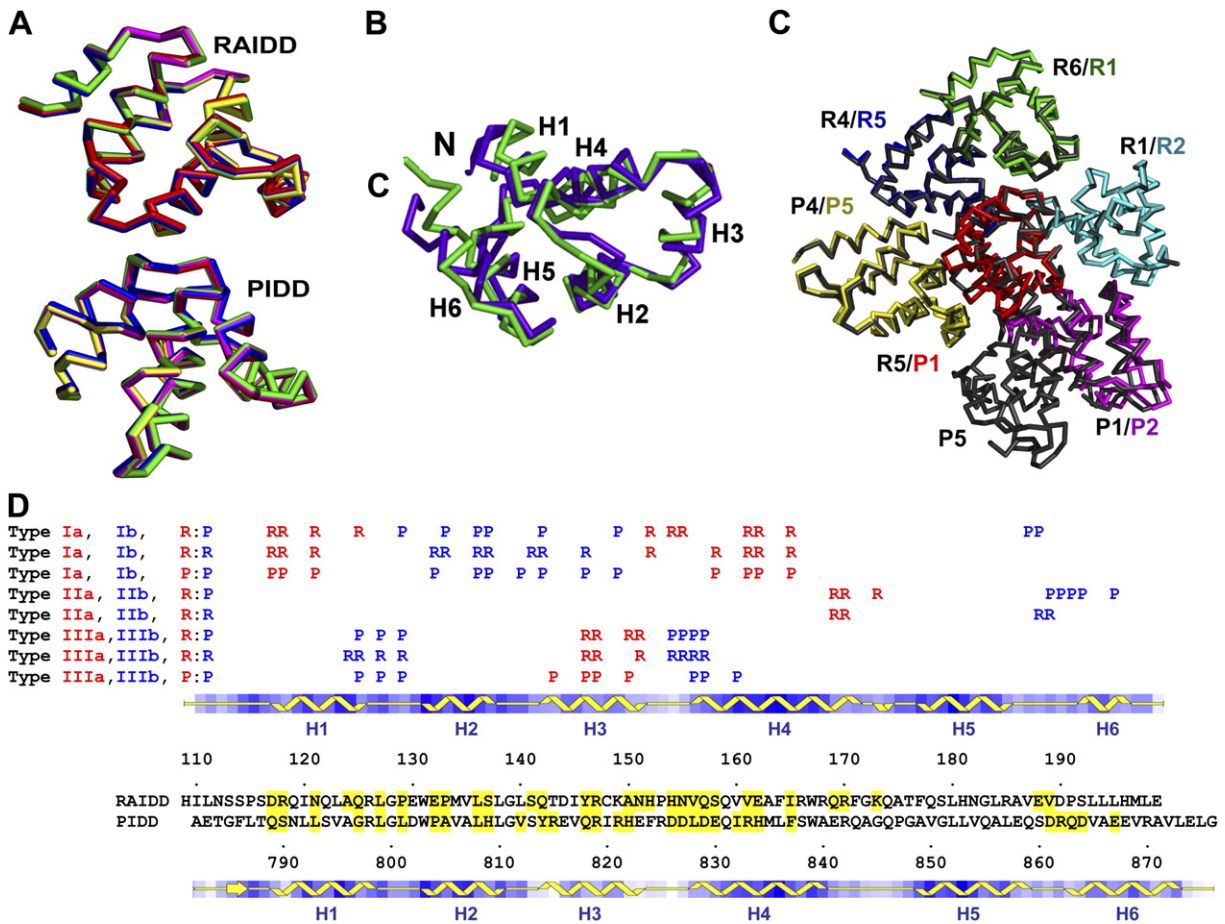


Figure 3. Quasi-Equivalent Environment

(A) Superposition of the five PIDD DD:RAIDD DD PR subcomplexes.
 (B) Superposition of RAIDD DD (purple) and PIDD DD (green).
 (C) Quasi-equivalence of the contacts on the plane of the staggered hexagonal construction. R5 and its neighboring DDs (gray) are superimposed with P1 and its neighboring DDs (different colors).
 (D) Structure-based sequence alignment between RAIDD DD and PIDD DD. Residues of RAIDD DD and PIDD DD involved in the eight different interfaces, which are classified into three types of interactions, are highlighted in yellow and marked. P, PIDD; R, RAIDD. Type Ia, IIa, and IIIa residues are marked in red, and type Ib, IIb, and IIIb residues are marked in blue.

the second DD (type Ib surface) (Figure 3D). In the first subtype of this type, the interaction is between a RAIDD DD and a PIDD DD molecule (R:P interaction) (Figure 4B). Many hydrophobic and polar interactions form the interface. Residues D117, V161, E162, and I165 of RAIDD pack against Y814 of PIDD. The side chains of R118 and N121 of RAIDD make hydrogen bonds, respectively, with the carbonyl oxygen and the side chain of H809 of PIDD. The side chain of Q125 of RAIDD forms a hydrogen bond with the main chain carbonyl oxygen of Q859 of PIDD. H154 and N155 of RAIDD interact with L801 of PIDD, and the side chain of N155 of RAIDD makes a hydrogen bond with the carbonyl oxygen of L801 of PIDD (Figure 4B). In the second subtype of this type, the PIDD DD is replaced by a RAIDD DD to generate the R:R interaction, and in the third subtype of this type of interaction,

the RAIDD DD is replaced by a PIDD DD to generate the P:P interaction (Figure 4B).

In the type II interaction, residues at the H4 helix and the H4-H5 loop of the first DD (type IIa surface) and residues at the H5-H6 loop and H6 helix of the second DD (type IIb surface) mediate this interaction (Figure 3D). In the first subtype of this type, the interaction is between the RAIDD DD and the PIDD DD in the PR subcomplexes (R:P interaction) (Figure 4C). The interface appears to be mostly polar and charged. Especially, there is a salt bridge interaction between D861 of PIDD and R170 of RAIDD; a hydrogen-bonding network between R862, N863, and D864 of PIDD and Q169 of RAIDD; and a hydrogen bond between the main chain of K173 of RAIDD and E867 of PIDD (Figure 4C). In the second subtype of this type, the PIDD DD is replaced by a RAIDD DD, and the interaction

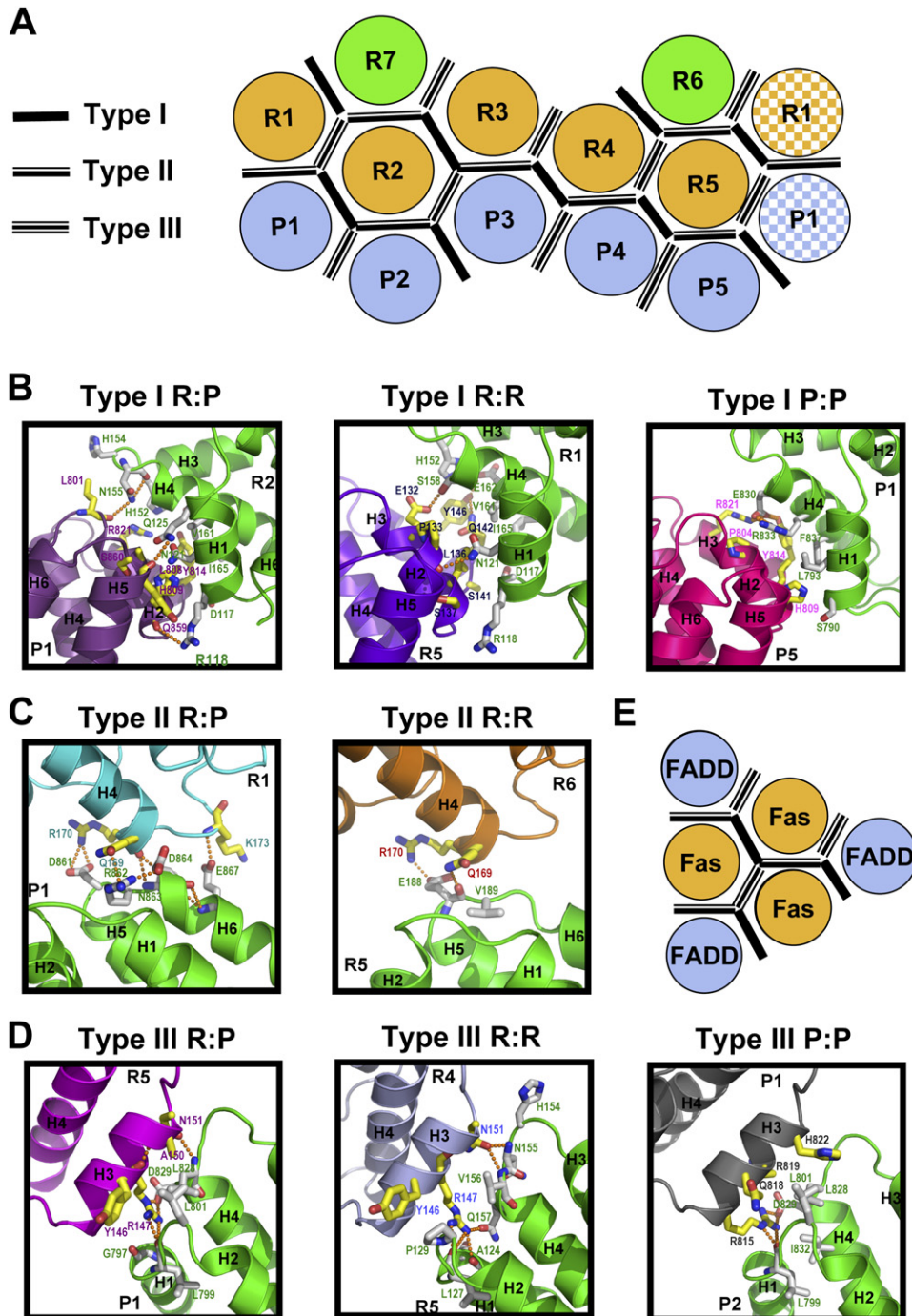


Figure 4. The Three Types of Interactions and Their Subtypes, a Total of Eight Interactions

(A) A schematic diagram for the locations of the three types of contacts in the PIDD DD:RAIDD DD complex.

(B) The three different subtypes of the type I interaction.

(C) The two different subtypes of the type II interaction.

(D) The three different subtypes of the type III interaction. Important residues and hydrogen bonding interactions are labeled.

(E) A hypothetical Fas DD:FADD DD complex constructed from the same three types of interactions. The same view is used as in (A), and the Fas DD:FADD DD complex may be considered as a portion of the PIDD DD:RAIDD DD complex composed of R7, R2, R3, P3, and R4.

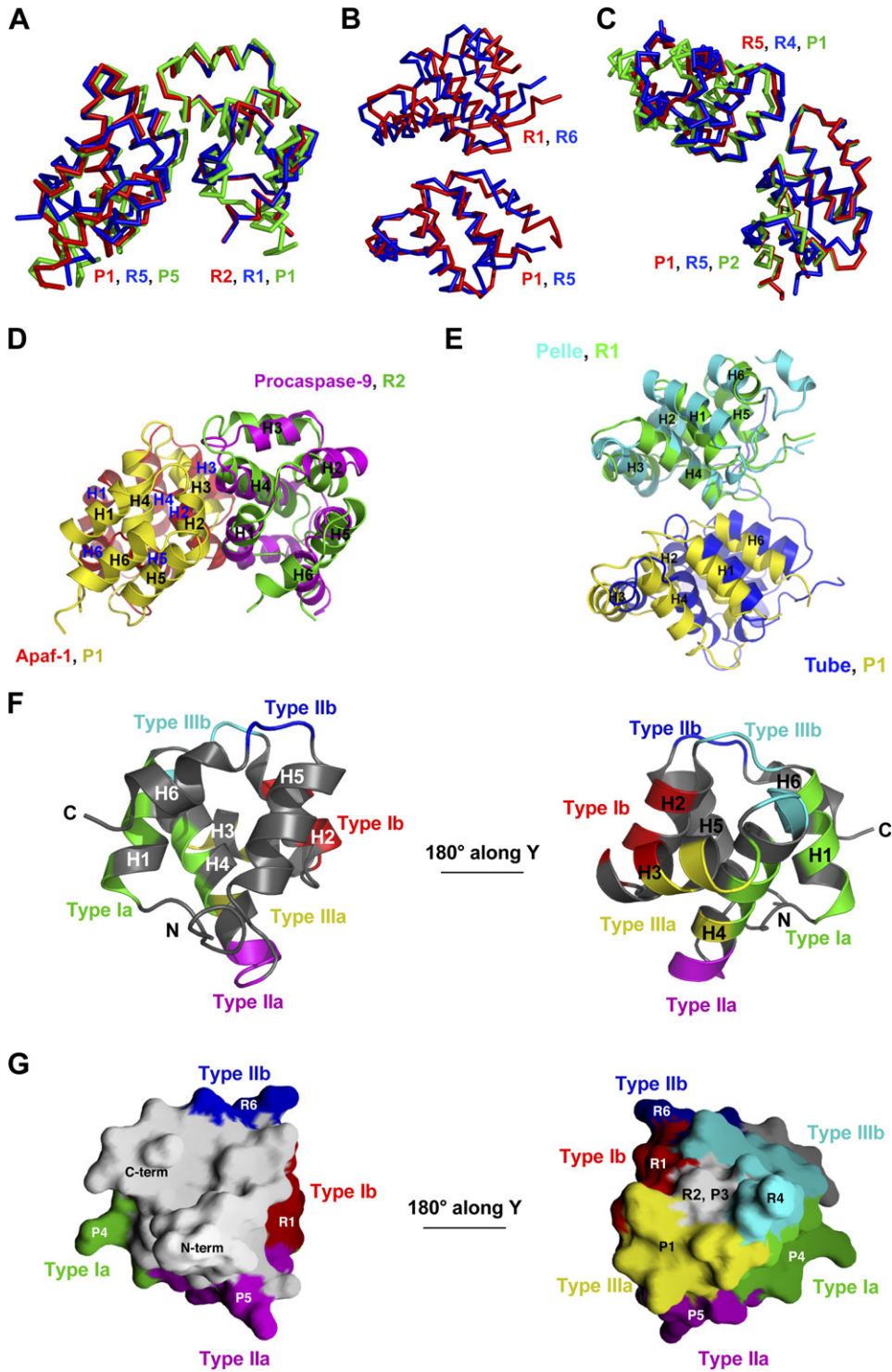


Figure 5. Conservation, Plasticity, and Coverage of the Type I, II, and III Interactions

(A) Comparison of the R:P (red), R:R (blue), and P:P (green) subtypes of the type I interaction. One molecule in each subtype is superimposed.
 (B) Comparison of the R:P (red) and R:R (blue) subtypes in the type II interaction. One molecule in each subtype is superimposed.
 (C) Comparison of the R:P (red), R:R (blue), and P:P (green) subtypes in the type III interaction. One molecule in each subtype is superimposed.
 (D) Comparison of the type I interaction (R2:P1) with the procaspase-9 CARD:Apaf-1 CARD interaction. R2 is superimposed with procaspase-9 CARD.
 (E) Comparison of the type II interaction (R1:P1) with the Pelle DD:Tube DD interaction. R1 is superimposed with Pelle DD.

is between two RAIDD DDs, such as those between R6 and R5 and between R7 and R2 (R:R interaction) (Figure 4C). This R:R interaction appears to be much less extensive than the corresponding R:P interaction.

In the type III interaction, residues at H3 of the first DD (type IIIa) interact with residues near the H1-H2 and the H3-H4 loops of the second DD (type IIIb) (Figure 3D). In the first subtype of this type, the interaction is between a RAIDD DD and a PIDD DD (R:P interaction) (Figure 4D). A mixture of hydrophobic, polar, and charged interactions occur at this interface, including the hydrophobic interaction between L801 of PIDD and Y146 of RAIDD, the salt bridge between D829 of PIDD and R147 of RAIDD, and a hydrogen bond between the main chain of L828 of PIDD and the side chain of N151 of RAIDD (Figure 4D). In the second subtype of this type, the PIDD DD is replaced by a RAIDD DD molecule (R:R interaction) (Figure 4D). In the third subtype of this type, the RAIDD DD is replaced by a PIDD DD molecule (P:P interaction) (Figure 4D).

Conservation, Plasticity, and Coverage of the Type I, II, and III Interactions in the DD Superfamily

Comparison among the different observations within each type revealed conservation, variation, and plasticity in these interactions. First, different observations within each subtype of interactions in the PIDD DD:RAIDD DD complex are completely conserved. In type I interactions, there are three observations of the R:P subtype, four observations of the R:R subtype, and two observations of the P:P subtype (Figure 4A). These are all conserved and align well to within RMSD of 0.4Å. Similar well-conserved alignment statistics are also observed within the five observations of the type II interaction R:P subtype, the two observations of the type II interaction R:R subtype, the two observations of the type III interaction R:P subtype, the five observations of the type III interaction R:R subtype, and the three observations of the type III interaction P:P subtype. These data suggest that each observed interaction is specific to the particular partners in the interaction.

Second, among the different interactions within each type, variations in orientations are observed. The different subtypes within each type of interaction in the PIDD DD:RAIDD DD complex show small adjustments in orientation (Figures 5A–5C). More significant adjustments are observed when the type I interaction in the PIDD DD:RAIDD DD complex is compared with the procaspase-9 CARD:Apaf-1 CARD interaction (Figure 5D) and when the type II interaction in the PIDD DD:RAIDD DD complex is compared with the Pelle DD:Tube DD complex (Figure 5E). Nonetheless, in all type I interactions, it is the H1 and H4 region of the first molecule (type Ia) interacting with the H2 and H3 region of the second molecule (type

Ib). In the type II interaction, however, the regions of contact are somewhat different. In addition to the common interaction between the H4-H5 region of the first DD and the H5-H6 region of the second DD, in the Pelle DD:Tube DD complex, the adjacent H2 region of the Pelle DD and the adjacent H1-H2 region of the Tube DD also participate in the interaction. In comparison with the type I interaction, the type II interaction buries a smaller surface area. In the Pelle DD:Tube DD complex, this interaction is strengthened by an additional interaction between a long tail of Tube and the H2-H3 and H4-H5 region of the Pelle DD. Therefore, depending on the exact partners in the complex, there is adjustment in orientation within each type of interactions. This structural plasticity may be important for accommodating the different sequences at these interfaces and for achieving specificity of different interaction pairs.

Not only are the regions of contacts relatively conserved, but the surface shape complementarity also appears to be preserved within each type of interaction. In type I interaction, the type Ia surface is concave and receives the convex surface of the type Ib surface. In both type II and type III interactions, the IIa and IIIa surfaces are convex, and the IIb and IIIb surfaces are concave. However, the nature of contacts is not conserved within each type of interaction. For example, in the procaspase-9 CARD:Apaf-1 CARD complex, the interacting surfaces are complementary in charge. In the analogous type I interactions in the PIDD DD:RAIDD DD complex, a complex network of hydrophobic contacts and hydrogen bonds mediate the interfaces.

The three types of interactions can coexist on a single DD, and each DD in the PIDD DD:RAIDD DD complex uses all types of surfaces to interact with neighboring DDs. Strikingly, when these interactions are mapped onto a particular DD (e.g., R5), the DD surface is almost all covered by these interactions, with the exception of the surface from which the termini protrude out (Figures 5F and 5G). In the standard orientation we use in this report, the DDs use type Ia and Ib surfaces to interact with other DDs above or below and use other types of surfaces for lateral interactions. The full coverage of these interactions on a DD and their conservation suggest that these three types of interaction may likely represent the major, if not all, modes of interactions in the DD superfamily.

Mutations that Disrupt the PIDD DD:RAIDD DD Interaction Prevent PIDDosome Formation and Caspase-2 Activation

To correlate the PIDD DD:RAIDD DD structure with PIDDosome function, we generated extensive structure-based mutations on all eight potential interfaces of the

(F) The six types of regions of R5 in its interaction with neighboring DDs in the complex. Two views of R5 are shown. Green and red: type Ia and Ib regions. Magenta and blue: type IIa and IIb regions. Yellow and cyan: type IIIa and IIIb regions.

(G) Surface representation of R5, showing the same six surfaces of contacts. Same color coding is used as in (F). The small gray area of surface at the 180° rotated view of R5 that does not contact any of the six immediate neighboring molecules interacts with R2 and P3 in the three-dimensional assembly.

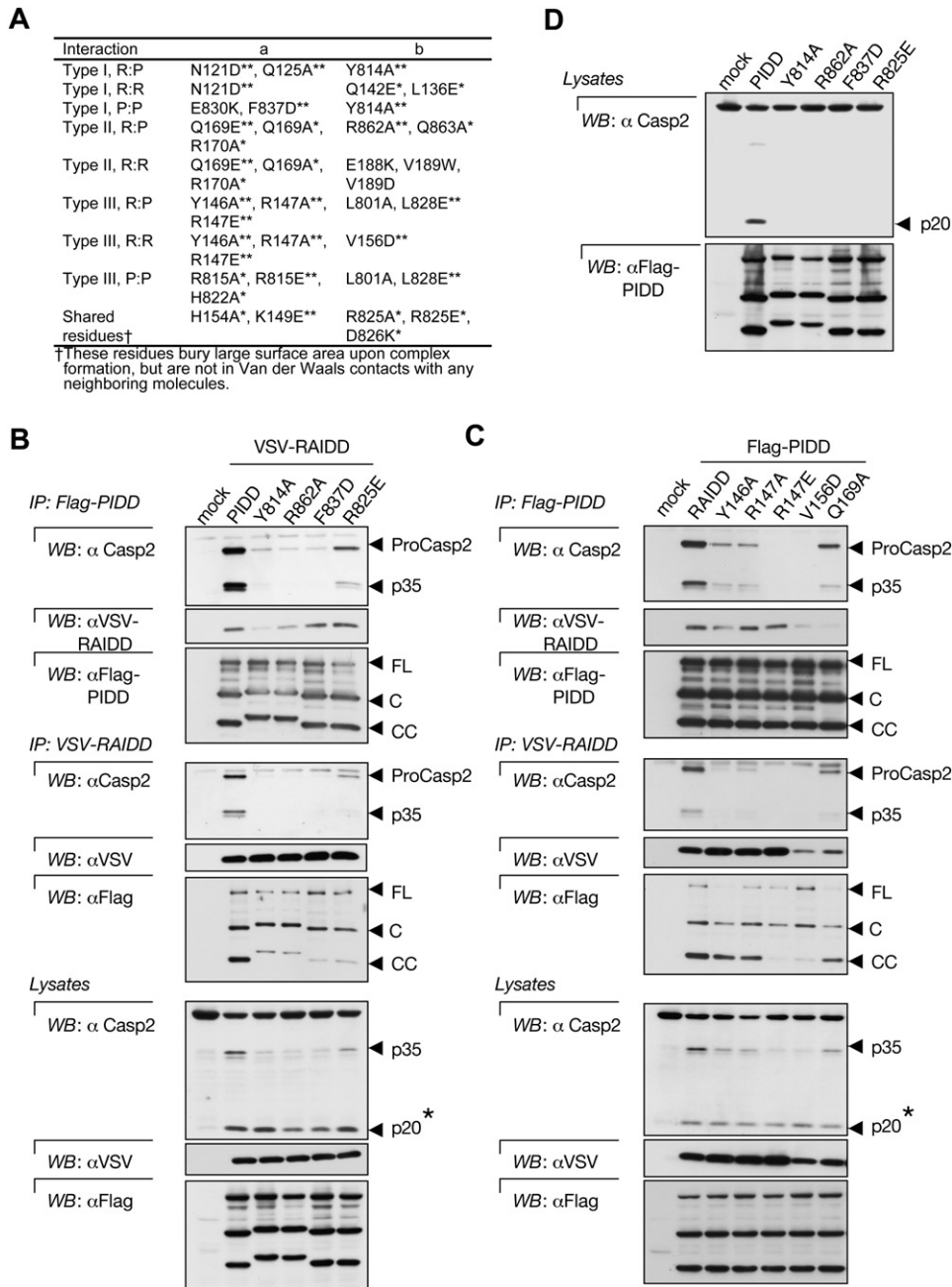


Figure 6. Mutational Analysis of the PIDD DD:RAIDD DD Interaction

(A) Structure-based mutations and their effects on assembly of the PIDD DD:RAIDD DD complex in vitro. Double and single asterisks show mutations that completely and partially disrupted complex formation, respectively.

(B) HEK293T cells were transiently transfected with expression vectors encoding wild-type or mutant Flag-PIIDD and wild-type VSV-RAIDD. PIDD or RAIDD was immunoprecipitated from the lysates with anti-Flag or anti-VSV antibodies, respectively, and coimmunoprecipitated proteins were revealed by Western blotting (WB). The asterisk corresponds to the p20 subunit of caspase-2, which is due the presence of overexpressed RAIDD (PIDD independent).

(C) Instead of PIDD mutants, the activity of RAIDD mutants was analyzed.

(D) As in (B), but PIDD proteins were expressed in the absence of overexpressed RAIDD.

three types and assayed complex formation (Figure 6A). We were able to obtain mutations on seven of the eight subtypes of interfaces that disrupted formation of the

PIDD DD:RAIDD DD complex, as judged by native gel electrophoresis and gel filtration chromatography (Figure S4). No intermediate complexes were observed for

any of the mutations. These data suggest that complex assembly may require the simultaneous presence of most, if not all, interfaces. We have so far not been able to obtain disruptive mutations on the R:R subtype of the type II interaction (Figure 6A), which mediates the assembly of R6 and R7 on the top layer.

We next investigated whether mutations at the PIDD DD:RAIDD DD interfaces would impact on PIDDosome formation and caspase-2 activation. To this end, several PIDD mutants were overexpressed in HEK293T cells along with wild-type RAIDD, and complex formation and caspase-2 activation were assessed by coimmunoprecipitation experiments after transient cotransfection (Figure 6B). While combined expression of the wild-type version resulted in formation of a complex containing PIDD (most likely the PIDD-CC form), RAIDD and active caspase-2, complex formation, and caspase-2 activation were either completely absent or attenuated with PIDD mutants. Several RAIDD mutants were also examined for their capacity to form the PIDDosome and shown to be defective (Figure 6C). Partial complex formation and caspase-2 activation were observed with several PIDD and RAIDD mutants, most of which also exhibited less drastic effects on PIDD DD:RAIDD DD interaction *in vitro* (Figure 6A). In addition, a complete absence of caspase-2 processing was seen with all PIDD mutants in the absence of RAIDD overexpression (using endogenous RAIDD) (Figure 6D). This indicates that caspase-2 recruitment and activation in the PIDDosome are critically dependent on the PIDD DD:RAIDD DD interaction we observe in the structure.

DISCUSSION

Molecular Mechanism of Caspase-2 Activation in the PIDDosome

Caspase activation is a hallmark of apoptotic cell death (Riedl and Shi, 2004; Salvesen, 2002). According to their sequence of activation, caspases may be divided into two groups: initiator caspases such as caspase-2, -8, -9, and -10, and effector caspases such as caspase-3 and -7 (Riedl and Shi, 2004; Salvesen, 2002). Unlike effector caspases, initiator caspases possess a domain of the DD superfamily at their N-terminal region for recruitment to oligomeric adaptor protein complexes upon apoptosis induction. Caspases are synthesized as single-chain procaspases, which undergo intrachain cleavage to generate the large and small subunits.

Caspases need to form specific dimers to be active. Because effector caspases are constitutive dimers, their activation is strictly a consequence of intrachain cleavage by initiator caspases. In contrast, intrachain cleavage does not appear to be the crucial factor for initiator caspase activation due to the relative longer lengths of the intersubunit linker regions. A proximity-induced dimerization model was proposed for initiator caspase activation because initiator caspases such as caspase-2, -8, and -9

are not constitutive dimers in solution, and specific homodimerization appears to be crucial for their activation (Baliga et al., 2004; Pop et al., 2006; Yin et al., 2006).

In agreement with this analysis, the different caspase-activating platforms are in different oligomerization states and may recruit caspases with different stoichiometry. While the mammalian apoptosome is a heptamer (Yu et al., 2005a), the *Drosophila* apoptosome is octameric (Yu et al., 2005b). CED4, the Apaf-1 homolog in *C. elegans*, is a tetramer (Yan et al., 2005). The DISC contains a trimer or likely multiple trimers, which may recruit three or more caspase-8 or caspase-10 molecules (Yang et al., 2005). Regardless of the stoichiometry, the key common event is oligomerization, which allows neighboring caspases to form specific activating dimers. This appears to be the case even when the oligomeric platform recruits odd numbers of caspases so that not all recruited caspases have dimeric partners. In this scenario, understanding caspase activation is reduced to understanding the oligomerization mechanisms of their activating complexes.

Therefore, it is not surprising that the PIDDosome brings seven caspase-2 molecules into proximity for their activation. One might ask why such an apparently unusual PIDD DD:RAIDD DD oligomerization platform is used to induce the proximity of caspase-2. Perhaps nature has evolved many different oligomerization platforms for caspase activation, and the PIDD DD:RAIDD DD complex is simply one of such examples. Upon recruitment to the PIDDosome, caspase-2 is able to form dimers and be activated, even in the absence of processing. The 50 residue linker region between the CARD and the catalytic region of caspase-2 likely facilitates dimerization in the correct orientations for caspase activation. Autoprocessing then proceeds, and caspase-2 dimerization and activity are both enhanced to induce mitochondrial events and cell death (Baliga et al., 2004; Read et al., 2002).

General Mechanisms of Interactions in the DD Superfamily

The DD superfamily is one of the largest and most widely distributed domain superfamilies. Evolutionarily, it seems that the ever-expanding DD superfamily may have evolved by inserting its domains into various signal transduction proteins such as caspases, kinases, and adaptor proteins. In this regard, it is amazing that almost all oligomeric signaling complexes in apoptosis and inflammation contain domains of the DD superfamily. For caspase-activating complexes, the DD superfamily domains may either be the major oligomerization platforms or the major mediators in recruiting the caspases. The DDs in the PIDDosome for caspase-2 activation and in the DISC for caspase-8 and caspase-10 activation fall into the former category, while the CARDS in the PIDDosome, DEDs in the DISC, and CARDS in the inflammasome fall into the latter category.

Our structure of the PIDD DD:RAIDD DD complex provides a glimpse of an oligomeric complex of the DD

superfamily and forms a template for other interactions in this superfamily. Because the RIP1 kinase DD is homologous to RAIDD DD, it is likely that the PIDD DD:RIP1 DD complex uses a similar assembly mechanism. In a much broader scenario, in contrast to the concept that the DD superfamily interactions may involve any available surfaces and may be very diverse, our study suggests that the observed three types of asymmetric interactions may represent preferred modes of interactions for DDs, and likely for the entire DD superfamily. This may be shown by the conservation between the type I interactions in the PIDD DD:RAIDD DD complex and the procaspase-9 CARD:Apaf-1 CARD interaction. In addition, in the DED1:DED2 interaction in the tandem DED-containing viral FLIP MC159, the H1 and H4 of DED2 interacts with H2 and H5 of DED1, which is somewhat similar to the type I interaction as well (Li et al., 2006; Yang et al., 2005).

Curiously, all these known interactions in the DD superfamily are asymmetric despite what might have been expected of homotypic interactions. This appears to be true for both effector recruitment, as in the procaspase-9 CARD:Apaf-1 CARD complex and the Pelle DD:Tube DD complex, and for oligomerization, as in the PIDD DD:RAIDD DD complex. This is not true, however, for secondary self-associations of DD superfamily domains that are involved in effector recruitment and are linked to oligomerization domains outside the DD superfamily. For example, Apaf-1 CARD is linked to a nucleotide-binding oligomerization domain (NOD). In the heptameric apoptosome, Apaf-1 NOD confers a 7-fold symmetry, and the Apaf-1 CARD also self-contacts with this symmetry in the presence of the NOD (Yu et al., 2005a).

On the subject of asymmetric interactions, an asymmetric trimeric model has also been proposed for the Fas DD:FADD DD complex (Weber and Vincenz, 2001). This model was generated from the structures of the Apaf-1 CARD:caspase-9 CARD complex (type I interaction) and the Pelle DD:Tube DD complex (type II interaction). When Pelle DD is superimposed with procaspase-9 CARD, the associated Tube DD and the Apaf-1 CARD pack against Pelle DD (or procaspase-9 CARD) in a well-organized trimer. The newly formed interaction between Tube DD and Apaf-1 CARD forms a different interface, which strikingly is very similar to the type III interaction observed in the PIDD DD:RAIDD DD complex. By continuing building interactions using these structures, a hexamer of DDs can be formed, in which the three central DDs may either be Fas DDs or FADD DDs (Figure 4E). Therefore, similar to the PIDD DD:RAIDD DD complex, the Fas DD:FADD DD complex may also be constructed from these three types of interfaces. In an independent experiment, type I, II, and III interactions were also found in docking models between Fas DD and FADD DD (Thakar et al., 2006).

The involvement of all three types of interactions in the assembly of various caspase-activating complexes is consistent with and explains the existing mutagenesis data on Fas (Huang et al., 1996; Martin et al., 1999), FADD (Hill et al., 2004), TNFR1 (Tartaglia et al., 1993; Telliez

et al., 2000b), and TRADD (Park and Baichwal, 1996). In each case, residues affecting the binding and/or function of the DD spread throughout its entire sequence. Similarly, our structure-based mutagenesis also identified important residues throughout the PIDD DD and RAIDD DD sequences (Figure 6A).

Asymmetry and the apparent preference for the three types of interactions may represent a unique feature of the homotypic interactions in the DD superfamily. One potentially strong rationale is that the conserved common fold of the DD superfamily members determines, or at least contributes to, the surface shape complementarity seen in all three types of asymmetric interactions. However, the nature of contacts may not be conserved within each type of interaction, as exemplified by the different surface hydrophobicity, hydrophilicity, and charge features of the different DDs (Park and Wu, 2006). In addition, as the major function of these domains is homotypic interaction, the interactions may have evolved from several primordial interaction pairs and be preserved through coevolution. Therefore, the preservation of these preferred interactions may reflect both fold conservation and evolutionary circumstances.

As the three types of interactions essentially cover a majority of the available surface of a DD (Figure 5G), it is likely that these three types of interactions represent the major, if not all, modes of interactions of the DD superfamily. For effector recruitment, only one of the three types of interactions is required. For oligomerization, it is likely that all three types of interactions are needed. The oligomerization stoichiometry is probably dictated by both the structural plasticity of the exact interaction pairs and how the interactions could be terminated. For the PIDD DD:RAIDD DD complex, the structure terminates within the layers as it forms rings. The top layer has only two RAIDD DD molecules, likely because of the two available spaces for interactions and the less extensive R:R subtype of the type II interaction (Figures 2E and 4A). The lower surfaces of the bottom layer of the PIDD DD molecules apparently have no affinity for either RAIDD DDs or PIDD DDs, therefore terminating the buildup of further layers. In the Fas DD:FADD DD complex, the inability of either FADD DD or Fas DD to associate with itself in the complex may leave the complex in a trimeric form. Given some plasticity at the interfaces, it is likely that, by choosing among the three types of interactions around each DD, a wide number of oligomeric complexes with different stoichiometry may be built. Selective usage of a certain type of interaction may even switch the binding to alternative DD adapters (Sandu et al., 2005). Therefore, these conserved asymmetric interactions may underlie the unique but elegant common assembly mechanism of the DD superfamily.

EXPERIMENTAL PROCEDURES

Protein Expression and Purification

The PIDD DD (residues 778–883) and RAIDD DD (residues 94–199) with C-terminal His tags were expressed in *E. coli* and purified using

the Ni-NTA affinity resin (Qiagen). They were then mixed and incubated at room temperature for 1 hr before being subjected to gel filtration chromatography using Superdex 200 HR 10/30 (GE Healthcare). The complex eluted at ~12 ml and was concentrated to 10–12 mg/ml.

MALS

The molar mass of the PIDD DD:RAIDD DD complex was determined by MALS. The complex was injected onto a Superdex 200 HR 10/30 gel filtration column (GE Healthcare) equilibrated in a buffer containing 20 mM Tris (pH 8.0) and 50 mM NaCl. The chromatography system was coupled to a three-angle light scattering detector (mini-DAWN EOS) and a refractive index detector (Optilab DSP) (Wyatt Technology). Data were collected every 0.5 s at a flow rate of 0.2 ml/min. Data analysis was carried out using the program ASTRA.

Electron Microscopy and Image Processing

PIDD DD:RAIDD DD complex was negatively stained with uranyl formate (Ohi et al., 2004). Images were recorded using low-dose conditions at a magnification of 52,000 \times and a defocus of $-1.5 \mu\text{m}$ with an FEI Tecnai T12 electron microscope operated at 120 kV. Two \times two pixels were averaged, yielding a pixel size of 2.69 Å. Using the SPIDER software (Frank et al., 1996), 3708 particles (from 16 images) were windowed into 80 \times 80 pixel images and subjected to ten cycles of multi-reference alignment and K-means classification specifying 25 classes. For comparison with the crystal structure, the atomic model was resolution filtered to 30 Å, and projections were calculated at 2° angular intervals. The reprojections were cross-correlated to the class averages, and the reprojections with the highest correlation coefficient were selected.

Structure Determination and Analysis

The assembled complex was crystallized at 20°C using 5.5% PEG 3350, 200 mM NaCl, and 100 mM Na/K phosphate (pH 6.5). To obtain a heavy atom derivative, the crystals were soaked with 1 mM 1,4-diacetoxymercuri-2,3-dimethoxybutane for 30 min. One crystal diffracted to 4.0 Å resolution, and a complete anomalous data set was collected at a wavelength of 1.0079 Å at the X4A beamline of NSLS. A 3.2 Å native data set was collected at the NE-CAT beamline of APS. Both data sets were processed using HKL2000 (Otwinowski and Minor, 1997).

The structure was determined by single-wavelength anomalous diffraction. There is a single partially surface-exposed free cysteine in the RAIDD DD structure (Park and Wu, 2006) and no cysteine in PIDD DD. Five strong mercury sites (15–20 σ) were found, and the structure was phased using the program SOLVE/RESOLVE (Terwilliger, 2004). A six-dimensional search of the electron density map using the RAIDD DD structure found ten DD molecules in the crystallographic asymmetric unit. The locations of the mercury sites and crystallographic refinement in CNS (Brunger et al., 1998) using the native data confirmed that five of the DD molecules were RAIDD DDs and that the five remaining molecules were PIDD DDs. Two additional RAIDD DD molecules were also found. The final atomic model contains seven RAIDD DDs and five PIDD DDs (Table 1). The structure was analyzed using O (Jones et al., 1991) and Pymol (DeLano Scientific).

Mutational Analysis of Complex Formation In Vitro

Site-directed mutagenesis was performed using the Quikchange kit (Stratagene) and confirmed by sequencing. Purified wild-type or mutant PIDD DD and RAIDD DD proteins were first mixed and incubated at room temperature for 1 hr. The mixed solutions were subjected to electrophoresis under native conditions on premade 8%–25% acrylamide gradient gels using the PhastSystem (GE Healthcare). The gels were stained with Coomassie blue, and complex formation was determined by the appearance of shifted bands. Mutational effects were also characterized by gel filtration chromatography using the Superdex 200 HR 10/30 column (GE Healthcare).

PIDDosome Formation and Caspase-2 Activation

PIDDosome formation was revealed by coimmunoprecipitation experiments after transient cotransfection of PIDD wild-type and RAIDD mutants or RAIDD wild-type and PIDD mutants. After 48 hr transfection, cells were lysed in lysis buffer containing 1% NP-40, 20 mM Tris (pH 7.4), 250 mM NaCl, 5% glycerol, and a protease inhibitor cocktail. After lysis, the extracts were incubated with anti-Flag or anti-VSV beads for 2 hr. After incubation the beads were washed four times with lysis buffer and analyzed by immunoblotting. The antibodies used for Western blotting were as follows: anti-caspase-2 11B4 (Apotech), mouse anti-VSV, and rabbit anti-Flag (Sigma).

Supplemental Data

The Supplemental Data include four supplemental figures and can be found with this article online at <http://www.cell.com/cgi/content/full/128/3/533/DC1/>.

ACKNOWLEDGMENTS

We thank Drs. David Eliezer, Olga Boudhka, and Fred Maxfield for helpful discussions; Randy Abramowitz and John Schwanof for data collection at X4A of NSLS; Kanagalaghatta Rajashankar and Igor Kourinov for data collection at NE-CAT of APS; Dr. Sally Kornbluth for providing the cDNA of human RAIDD; Dr. Jin Kuk Yang for help with data collection; Jin Wu for maintaining X-ray equipment and computers; Su-Chang Lin for help with the light scattering experiment; and the Wu lab members for discussions. The molecular EM facility at Harvard Medical School was established with a generous donation from the Giovanni Armenise Harvard Center for Structural Biology and is maintained with funds from the NIH.

Received: November 23, 2006

Revised: December 25, 2006

Accepted: January 6, 2007

Published: February 8, 2007

REFERENCES

- Baliga, B.C., Read, S.H., and Kumar, S. (2004). The biochemical mechanism of caspase-2 activation. *Cell Death Differ.* 11, 1234–1241.
- Bergeron, L., Perez, G.I., Macdonald, G., Shi, L., Sun, Y., Jurisicova, A., Varmuza, S., Latham, K.E., Flaws, J.A., Salter, J.C., et al. (1998). Defects in regulation of apoptosis in caspase-2-deficient mice. *Genes Dev.* 12, 1304–1314.
- Brunger, A.T., Adams, P.D., Clore, G.M., DeLano, W.L., Gros, P., Grosse-Kunstleve, R.W., Jiang, J.S., Kuszewski, J., Nilges, M., Pannu, N.S., et al. (1998). Crystallography & NMR system: A new software suite for macromolecular structure determination. *Acta Crystallogr. D Biol. Crystallogr.* 54, 905–921.
- Duan, H., and Dixit, V.M. (1997). RAIDD is a new 'death' adaptor molecule. *Nature* 385, 86–89.
- Frank, J., Radermacher, M., Penczek, P., Zhu, J., Li, Y., Ladjadj, M., and Leith, A. (1996). SPIDER and WEB: Processing and visualization of images in 3D electron microscopy and related fields. *J. Struct. Biol.* 116, 190–199.
- Guo, Y., Srinivasula, S.M., Druilhe, A., Fernandes-Alnemri, T., and Alnemri, E.S. (2002). Caspase-2 induces apoptosis by releasing proapoptotic proteins from mitochondria. *J. Biol. Chem.* 277, 13430–13437.
- Hill, J.M., Morisawa, G., Kim, T., Huang, T., Wei, Y., and Werner, M.H. (2004). Identification of an expanded binding surface on the FADD death domain responsible for interaction with CD95/Fas. *J. Biol. Chem.* 279, 1474–1481.

- Huang, B., Eberstadt, M., Olejniczak, E.T., Meadows, R.P., and Fesik, S.W. (1996). NMR structure and mutagenesis of the Fas (APO-1/CD95) death domain. *Nature* **384**, 638–641.
- Janssens, S., Tinel, A., Lippens, S., and Tschopp, J. (2005). PIDD mediates NF- κ B activation in response to DNA damage. *Cell* **123**, 1079–1092.
- Jones, T.A., Zou, J.-Y., Cowan, S.W., and Kjeldgaard, M. (1991). Improved methods for building models in electron density maps and the location of errors in those models. *Acta Crystallogr. A* **47**, 110–119.
- Kohl, A., and Grutter, M.G. (2004). Fire and death: The pyrin domain joins the death-domain superfamily. *C. R. Biol.* **327**, 1077–1086.
- Lassus, P., Opitz-Araya, X., and Lazebnik, Y. (2002). Requirement for caspase-2 in stress-induced apoptosis before mitochondrial permeabilization. *Science* **297**, 1352–1354.
- Li, F.Y., Jeffrey, P.D., Yu, J.W., and Shi, Y. (2006). Crystal structure of a viral FLIP: Insights into FLIP-mediated inhibition of death receptor signaling. *J. Biol. Chem.* **281**, 2960–2968.
- Lin, Y., Ma, W., and Benchimol, S. (2000). Pidd, a new death-domain-containing protein, is induced by p53 and promotes apoptosis. *Nat. Genet.* **26**, 122–127.
- Martin, D.A., Zheng, L., Siegel, R.M., Huang, B., Fisher, G.H., Wang, J., Jackson, C.E., Puck, J.M., Dale, J., Straus, S.E., et al. (1999). Defective CD95/APO-1/Fas signal complex formation in the human autoimmune lymphoproliferative syndrome, type Ia. *Proc. Natl. Acad. Sci. USA* **96**, 4552–4557.
- Ohi, M., Li, Y., Cheng, Y., and Walz, T. (2004). Negative staining and image classification—Powerful tools in modern electron microscopy. *Biol. Proced. Online* **6**, 23–34.
- Otwinowski, Z., and Minor, W. (1997). Processing of X-ray diffraction data collected in oscillation mode. *Methods Enzymol.* **276**, 307–326.
- Park, A., and Baichwal, V.R. (1996). Systematic mutational analysis of the death domain of the tumor necrosis factor receptor-1-associated protein TRADD. *J. Biol. Chem.* **271**, 9858–9862.
- Park, H.H., and Wu, H. (2006). Crystal structure of RAIDD death domain implicates potential mechanism of PIDDosome assembly. *J. Mol. Biol.* **357**, 358–364.
- Park, H.H., Lo, Y.C., Lin, S.C., Wang, L., Yang, J.K., and Wu, H. (2007). The death domain superfamily in intracellular signaling of apoptosis and inflammation. *Annu. Rev. Immunol.* **25**, 561–586.
- Pick, R., Badura, S., Bossler, S., and Zornig, M. (2006). Upon intracellular processing, the C-terminal death domain-containing fragment of the p53-inducible PIDD/LRDD protein translocates to the nucleoli and interacts with nucleolin. *Biochem. Biophys. Res. Commun.* **349**, 1329–1338.
- Pop, C., Timmer, J., Sperandio, S., and Salvesen, G.S. (2006). The apoptosome activates caspase-9 by dimerization. *Mol. Cell* **22**, 269–275.
- Qin, H., Srinivasula, S.M., Wu, G., Fernandes-Alnemri, T., Alnemri, E.S., and Shi, Y. (1999). Structural basis of procaspase-9 recruitment by the apoptotic protease-activating factor 1. *Nature* **399**, 549–557.
- Read, S.H., Baliga, B.C., Ekert, P.G., Vaux, D.L., and Kumar, S. (2002). A novel Apaf-1-independent putative caspase-2 activation complex. *J. Cell Biol.* **159**, 739–745.
- Reed, J.C., Doctor, K.S., and Godzik, A. (2004). The domains of apoptosis: A genomics perspective. *Sci. STKE* **2004**, re9.
- Riedl, S.J., and Shi, Y. (2004). Molecular mechanisms of caspase regulation during apoptosis. *Nat. Rev. Mol. Cell Biol.* **5**, 897–907.
- Robertson, J.D., Enoksson, M., Suomela, M., Zhivotovsky, B., and Orrenius, S. (2002). Caspase-2 acts upstream of mitochondria to promote cytochrome c release during etoposide-induced apoptosis. *J. Biol. Chem.* **277**, 29803–29809.
- Salvesen, G.S. (2002). Caspases and apoptosis. *Essays Biochem.* **38**, 9–19.
- Sandu, C., Gavathiotis, E., Huang, T., Wegorzewska, I., and Werner, M.H. (2005). A mechanism for death receptor discrimination by death adaptors. *J. Biol. Chem.* **280**, 31974–31980.
- Tartaglia, L.A., Ayres, T.M., Wong, G.H., and Goeddel, D.V. (1993). A novel domain within the 55 kd TNF receptor signals cell death. *Cell* **74**, 845–853.
- Telliez, J.B., Bean, K.M., and Lin, L.L. (2000a). LRDD, a novel leucine rich repeat and death domain containing protein. *Biochim. Biophys. Acta* **1478**, 280–288.
- Telliez, J.B., Xu, G.Y., Woronicz, J.D., Hsu, S., Wu, J.L., Lin, L., Sukits, S.F., Powers, R., and Lin, L.L. (2000b). Mutational analysis and NMR studies of the death domain of the tumor necrosis factor receptor-1. *J. Mol. Biol.* **300**, 1323–1333.
- Terwilliger, T. (2004). SOLVE and RESOLVE: Automated structure solution, density modification and model building. *J. Synchrotron Radiat.* **11**, 49–52.
- Thakar, J., Schleinkofer, K., Borner, C., and Dandekar, T. (2006). RIP death domain structural interactions implicated in TNF-mediated proliferation and survival. *Proteins* **63**, 413–423.
- Tinel, A., and Tschopp, J. (2004). The PIDDosome, a protein complex implicated in activation of caspase-2 in response to genotoxic stress. *Science* **304**, 843–846.
- Tinel, A., Janssens, S., Lippens, S., Cuenin, S., Logette, E., Jaccard, B., Quadroni, M., and Tschopp, J. (2007). Autoproteolysis of PIDD marks the bifurcation between pro-death caspase-2 and pro-survival NF- κ B pathway. *Embo J.* **26**, 197–208. Published online December 7, 2006. 10.1038/sj.emboj.7601473.
- Wang, L., Miura, M., Bergeron, L., Zhu, H., and Yuan, J. (1994). Ich-1, an Ice/ced-3-related gene, encodes both positive and negative regulators of programmed cell death. *Cell* **78**, 739–750.
- Weber, C.H., and Vincenz, C. (2001). A docking model of key components of the DISC complex: Death domain superfamily interactions redefined. *FEBS Lett.* **492**, 171–176.
- Xiao, T., Towb, P., Wasserman, S.A., and Sprang, S.R. (1999). Three-dimensional structure of a complex between the death domains of Pelle and Tube. *Cell* **99**, 545–555.
- Yan, N., Chai, J., Lee, E.S., Gu, L., Liu, Q., He, J., Wu, J.W., Kokel, D., Li, H., Hao, Q., et al. (2005). Structure of the CED-4-CED-9 complex provides insights into programmed cell death in *Caenorhabditis elegans*. *Nature* **437**, 831–837.
- Yang, J.K., Wang, L., Zheng, L., Wan, F., Ahmed, M., Lenardo, M.J., and Wu, H. (2005). Crystal structure of MC159 reveals molecular mechanism of DISC assembly and FLIP inhibition. *Mol. Cell* **20**, 939–949.
- Yin, Q., Park, H.H., Chung, J.Y., Lin, S.C., Lo, Y.C., da Graca, L.S., Jiang, X., and Wu, H. (2006). Caspase-9 holoenzyme is a specific and optimal procaspase-3 processing machine. *Mol. Cell* **22**, 259–268.
- Yu, X., Acehan, D., Menetret, J.F., Booth, C.R., Ludtke, S.J., Riedl, S.J., Shi, Y., Wang, X., and Akey, C.W. (2005a). A structure of the human apoptosome at 12.8 Å resolution provides insights into this cell death platform. *Structure* **13**, 1725–1735.
- Yu, X., Wang, L., Acehan, D., Wang, X., and Akey, C.W. (2005b). Three-dimensional structure of a double apoptosome formed by the *Drosophila* Apaf-1 related killer. *J. Mol. Biol.* **355**, 577–589.

Accession Numbers

The coordinates have been deposited in the RCSB Protein Data Bank with the PDB code 2OF5.

Supplemental Data

Death Domain Assembly Mechanism

Revealed by Crystal Structure of

the Oligomeric PIDDosome Core Complex

Hyun Ho Park, Emmanuelle Logette, Stefan Raunser, Solange Cuenin, Thomas Walz, Jurg Tschopp, and Hao Wu

Figure S1. Negative Stain Electron Microscopy of the PIDD DD: RAIDD DD Complex

(A) The raw images revealed that the complexes were monodisperse and homogeneous in size. Scale bar is 100 nm.

(B) The class averages obtained by classifying 3,708 particles into 25 classes showed different projection views of the PIDD DD: RAIDD DD complex indicating that it adsorbed to the grid in different orientations. Scale bar is 10 nm.

(C) Representative class averages (top row) obtained with negatively stained sample. Each class contains 50-170 particles. Scale bar is 10 nm. The class averages represent different views of the PIDD DD: RAIDD DD complex as shown by the corresponding re-projections from the crystal structure resolution-filtered to 30 Å (bottom row). The orientations of the complex corresponding to the experimental projections (top row) and calculated re-projections (bottom row) are shown with the 30 Å resolution-filtered model in the middle row.

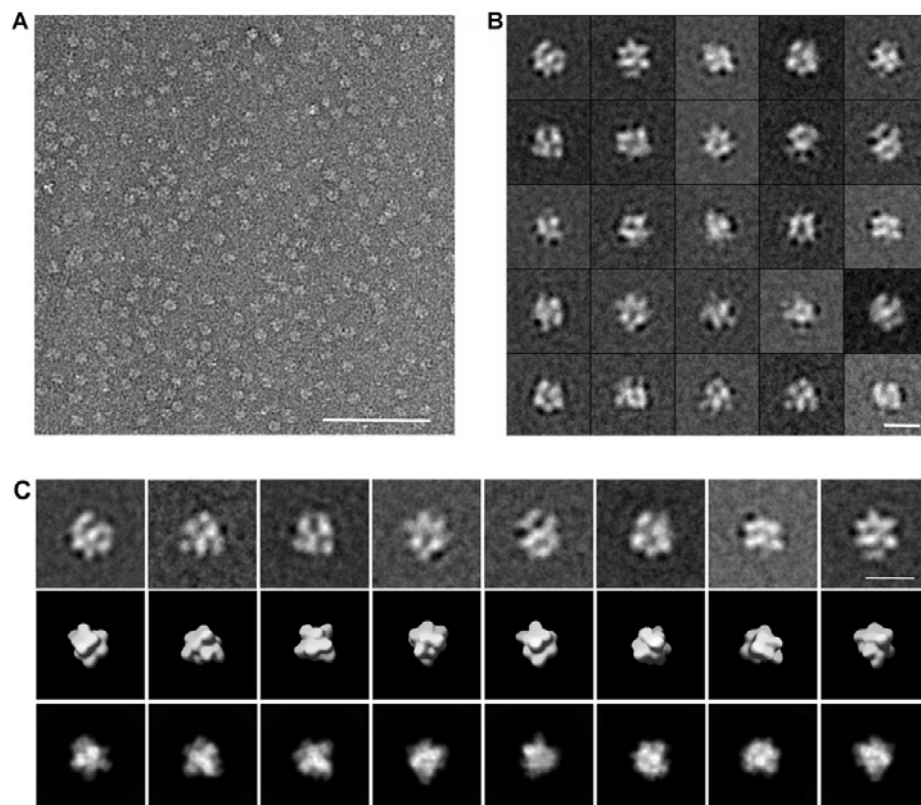
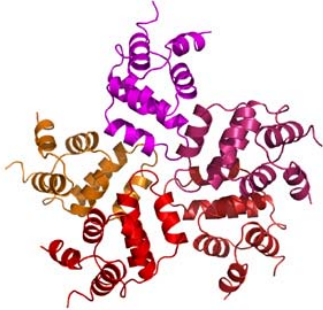


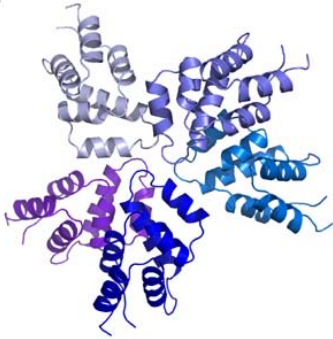
Figure S2. Middle and Bottom Layers of the Complex

(A and C) Top and side views of the middle layer of RAIDD DD. (B and D) Top and side views of the bottom layer of PIDD DD.

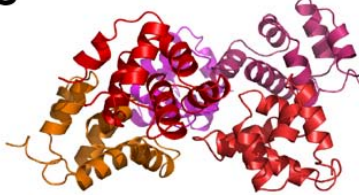
A



B



C



D

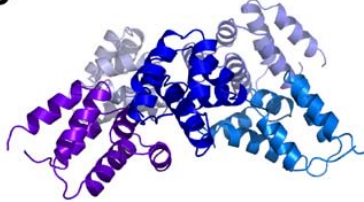


Figure S3. Quasi-Equivalence of the Assembly

(A–D) Superpositions of P2–P5 and their respective neighboring DDs with R5 and its neighboring DDs.

(E–J) Superpositions of R1–R4, R6–R7 and their respective neighboring DDs with R5 and its neighboring DDs.

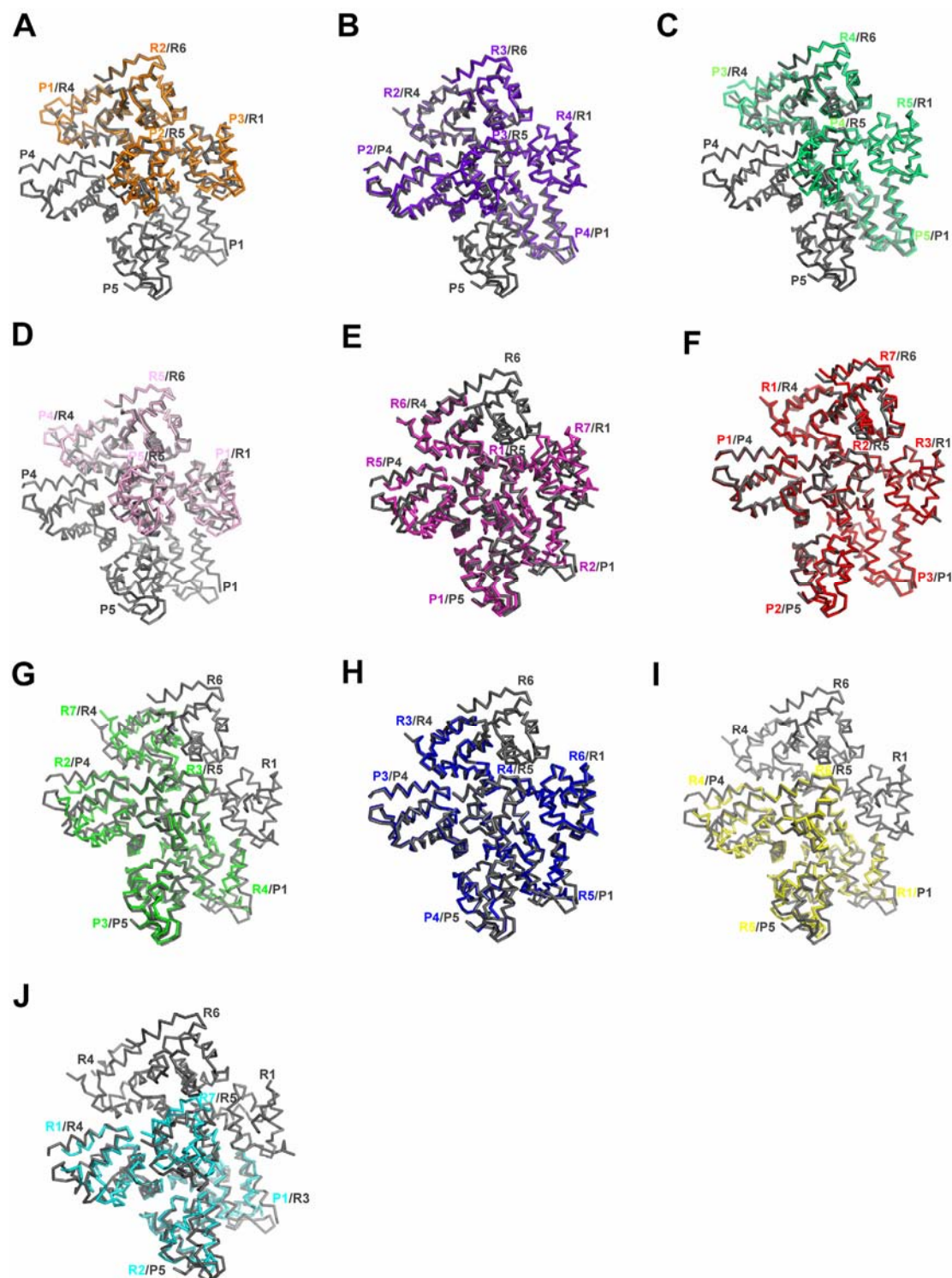


Figure S4. Gel Filtration Analysis of Selective PIDD DD and RAIDD DD Mutants in Complex Formation

Approximately equal amounts of a PIDD DD mutant (Y814A, R862A, F837D or R825E) and the wild-type RAIDD DD were mixed. Similarly, approximately equal amounts of a RAIDD DD mutant (Y146A or R147E) and the wild-type PIDD DD were mixed. Both types of mixtures were subjected to gel filtration chromatography using the Superdex 200 HR 10/30 column. The chromatographic trace for the mixture of the wild-type RAIDD DD and the wild-type PIDD DD is also shown.

